Available online at www.sciencedirect.com
SCIENCE DIRECT
Journal of Photochemistry and Photobiology A: Chemistry 179 (2006) 75–80
Journal of Photochemistry and Photobiology A:Chemistry
www.elsevier.com/locate/jphotochem

Microporous SiO_2–TiO_2 nanosols pillared montmorillonite for photocatalytic decomposition of methyl orange

Song Liu [a,b,*], Jae-Hun Yang [a], Jin-Ho Choy [a,**]

[a] *National Nanohybrid Materials Laboratory, School of Chemistry and Molecular Engineering, Seoul National University, 151-747 Seoul, South Korea*
[b] *College of Chemistry, South China University of Technology, Guangzhou 510640, PR China*

Received 9 February 2005; received in revised form 14 July 2005; accepted 22 July 2005
Available online 22 August 2005

Abstract

Layered nanohybrid, SiO_2–TiO_2 sol pillared clay, has been prepared by ion exchange reaction of the sodium ion in montmorillonite with positively charged SiO_2–TiO_2 sol particles. From powder X-ray diffraction (XRD), the basal spacing (d_{001}) of sample calcined at 400 °C was found to be 4.65 nm, due to the multistacking of nanosized SiO_2 and TiO_2 sol particles, which was confirmed by micropore analysis calculated from nitrogen adsorption. The BET specific surface area shows the value of 446 m^2/g and total porosity is found to be 0.28 ml/g, and the pores are mainly composed of micropore with a size of ca. 1.1 nm. TiO_2 particles stabilized in the interlayer space of montmorillonite are found to be quantum size according to UV–vis spectroscopy. The photocatalytic properties of the SiO_2–TiO_2 pillars were investigated in the degradation of methyl orange in water. The optimal photocatalyst amount is 55 mg/l with the reaction rate constant being 0.33 h^{-1}. The presence of iron ions dopants does not influence or is detrimental for the occurrence of methyl orange photodegradation.

Keywords: Photocatalysis; Pillared clay; Methyl orange; Iron ion doping; Titania

1. Introduction

Heterogeneous photocatalysis using TiO_2 has been considered as effective technology for treating refractory organic compound in water and in air. The photocatalytic efficiency of TiO_2 is greatly influenced by crystal structure, particle size, surface area, and porosity, as determined by different methods. Increasing the photocatalyst surface area and reducing the dimension photocatalyst to nanometer-size are the obvious means of improving the efficiency of photocatalytic oxidation reaction [1].

It is well known pillared clays have a structure in which parallel two-dimension silicate layers of the clay are supported with small particles of metal oxide and micro- to mesopores is formed. Pillared clays can provide large surface and pore volumes, which are beneficial for organic compounds and intermediates to reach and leave the active sites on the surface. In addition, the size of the metal oxide pillars incorporated between the silicate layers is of nanometer dimension [2–6]. The SiO_2–TiO_2 pillared clay is especially interesting because the possibility to obtain the small size TiO_2 particles below 5 nm stabilized in the interlayer space of montmorillonite, having higher photocatalytic activities than bulk ones [7–9]. Since the pore size and internal surface area of pillared clays are strongly depend upon the nature of pillaring agents and pillaring condition, it is necessary to set up new strategies to design tailor-making pillared materials by controlling the pillaring parameters.

In the study, utilizing formation of nanometer-sized SiO_2–TiO_2 sols aggregates in acidic solution, we attempted to synthesize the nanohybrid with multistacked SiO_2–TiO_2 sol particles between montmollonite layers and to understand the interlayer structure. The SiO_2–TiO_2 pillared clay was modified by iron ions doping. Photoactivity of the catalyst is evaluated using the photocatalytic oxidation of methyl orange as the test reaction.

* Corresponding author. Tel.: +86 20 87114875; fax: +86 20 87112906.
** Corresponding author.
E-mail address: chsliu@scut.edu.cn (S. Liu).

1010-6030/$ – see front matter © 2005 Elsevier B.V. All rights reserved.
doi:10.1016/j.jphotochem.2005.07.016

2. Experimental

2.1. Materials

The natural Na-montmorillonite (Kunipia F, Kunimine Industry, Japan) with the chemical formula of $(Na_{0.35}K_{0.01}Ca_{0.02})(Si_{3.89}Al_{0.11})(Al_{1.60}Fe_{0.08}Mg_{0.32})O_{10}(OH)_2{\cdot}nH_2O$ and the cation exchange capacity (CEC) of 100 meq./100 g was used as starting material. A 1 wt% aqueous suspension of montmollonite was preswelled for 1 day before ion exchange reaction. All other reagents were of analytical grade (Aldrich).

2.2. Preparation

A silica sol solution was prepared by mixing $Si(OC_2H_5)_4$, 2 M HCl, and ethanol with a ratio of 41.6 g/10 ml/12 ml at room temperature for 2 h. Titanium tetrachloride was also hydrolyzed by adding it into 1 M HCl solution with a molar ratio of $HCl/TiCl_4 = 6$, and the resulting translucent slurry was aged to a clear sol solution by continuous stirring for 1 h at room temperature. Finally, the silica sol solution and titania solution were intermixed with a ratio of Si/Ti = 10/1, and the mixture was stirred further for 1 h at room temperature the used for pillaring reaction.

The ion exchange reaction was carried out by titrating the mixed solution into clay suspension with a ratio of Si/Ti/clay = 20 mmol/2 mmol/1 g. The mixture was allowed to stand for 5 h at 60 °C, to exchange the Na^+ ions with the mixed SiO_2 and TiO_2 sol particles completely. The products were separated by centrifugation, washed with the mixed solution of ethanol and water (1:1, v/v) for six times to remove the excess sols, and then freezing dried. The dried samples were finally calcined for 3 h at 400 °C (abbreviated hereafter as PILC).

Iron-doped pillared clay powders were prepared by incipient wetness impregnation method of pillared clay, using aqueous solutions of $Fe(NO_3)_3$ containing the required nominal quantity of Fe^{3+} ions; While the mixture was carefully stirred, the solvent was slowly evaporation, the samples were dried at 100 °C for 4 h, and fired at 400 °C for 6 h (name hereafter *X* Fe/PILC, *X* is the weight iron percent in the SiO_2–TiO_2 pillared clay). For comparison, a sample of PILC was also fired at 400 °C for 6 h (abbreviated as THPILC).

2.3. Characterization

Powder X-ray diffraction (XRD) patterns for orientated samples were recorded using a Philips PW1830 diffractometer with Ni-filtered Cu Kα radiation (λ = 0.154056 nm). Elemental analyses of pillared clay were carried out with the inductively coupled plasma (ICP:Shimazu ICP-5000), for which the samples were fused with lithium metaborate at 900 °C and dissolved in 3% HNO_3 solution.

Diffuse reflectance UV–vis spectra were recorded on a Perkin-Elmer Lambda 12 spectrometer equipped with an integrating sphere of 60 mm in diameter using $BaSO_4$ as a standard.

Nitrogen adsorption–desorption isotherm was measured volumetrically at the liquid nitrogen temperature with a home-made computer-controlled measurement system. The calcined sample was degassed at 250 °C for 2 h under vacuum prior to adsorption measurement.

2.4. Photoreactivity measurements

Irradiations were performed at room temperature using a xenon lamp (SVX 1530, 300 W) with a 12 cm water filter to remove IR irradiation. The integrated light intensity between 300 and 800 nm was about 80 mW/cm^2. The photochemical reactor was a Pyrex glass vessel with a flat quartz window (2.5 cm in diameter) for light illumination. For each experiment, photocatalyst was added to 100 ml of 0.01 mM methyl orange solution stirred with a magnetic stirrer, and air was bubbled through the reaction media during the experiments. Before irradiation, suspensions were stirred for 3 h in the dark to ensure equilibrium of the solution with photocatalyst. The concentration of aqueous methyl orange was determined with a Perkin-Elmer Lambda 12 spectrometer by measuring the absorbance at 464 nm.

3. Results and discussion

3.1. Chemical analysis

Assuming that the chemical composition of aluminosilicate layer is unchanged during the pillaring reaction, the chemical composition of pillared product can be determined as $[Si_{7.36}O_{14.72}Ti_{0.49}O_{0.98}](Si_{3.89}Al_{0.11})(Al_{1.60}Fe_{0.08}Mg_{0.32})O_{10}(OH)_2$.

3.2. Powder X-ray diffraction analysis

As shown in Fig. 1, the d_{001} peaks and of powder XRD patterns of PILC and Fe/PILC had similar shapes and positions. This result indicates that the intercalated structure of pillared clay is maintained during the doping treatment. The basal spacing (d_{001}) of sample was found to be 4.65 nm with its gallery height of 3.69 nm by subtracting the thickness of the aluminosilicate layer (0.96 nm) from its basal spacing. There was no diffraction peaks assignable to Fe_2O_3 in iron-doped pillared clay and there was no diffraction peaks assignable to TiO_2 in all the samples. It can be seen that PILC has only 4.6 wt% TiO_2, which may be not enough to generate anatase phase.

3.3. Nitrogen adsorption–desorption isotherm

The N_2 adsorption–desorption isotherm shown in Fig. 2, characterized by Type IV according to the BDDT classification, exhibits relatively large hysteresis whose loop

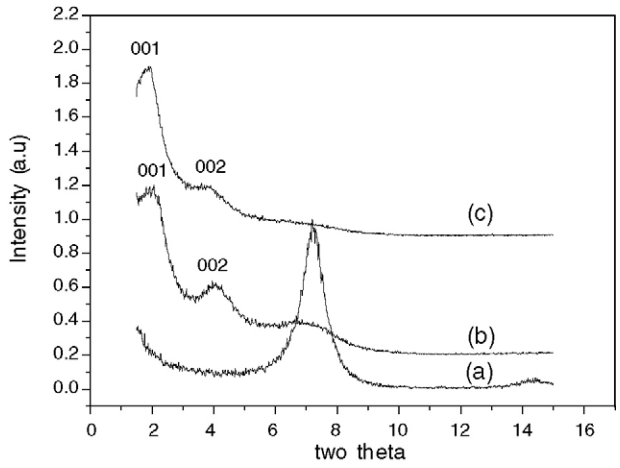

Fig. 1. Powder X-ray diffraction pattern for (a) montmorillonite, (b) PILC, and (c) 3.584 Fe/PILC.

is of Type B in de Boer's five types [10,11], indicating the presence of open slit-shaped capillaries with very wide bodies and narrow short necks. The BET specific surface area and porosity are found to be 446 m^2/g and 0.28 ml/g, respectively.

Micropore was analyzed by MP method [11] as shown in Fig. 3. According to the MP method, the total porosity of pillared clay was found to be mainly composed of the micropore (0.22 ml/g) with an average pore size of ca. 1.1 nm though its gallery height was in the size of mesopore. This indicates that pillared clay is the nanohybrid with multistacked SiO_2–TiO_2 sol particles between the layers of montmorillonite.

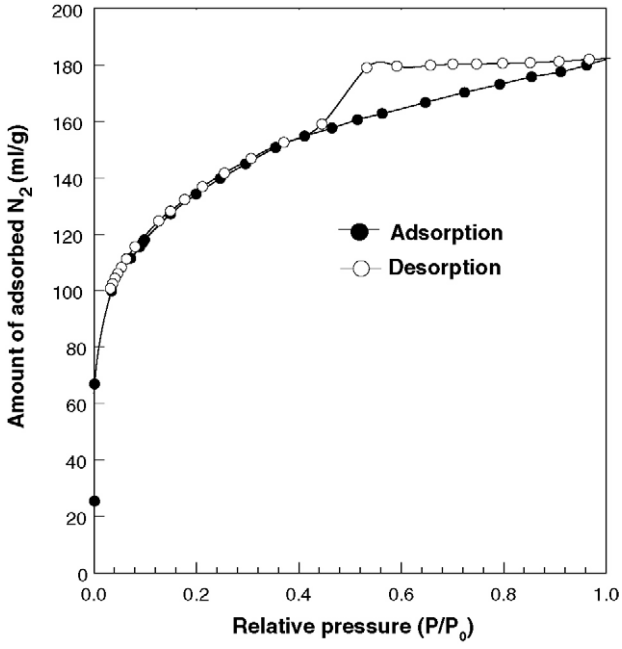

Fig. 2. Nitrogen adsorption–desorption isotherm for SiO_2–TiO_2 pillared montmorillonite.

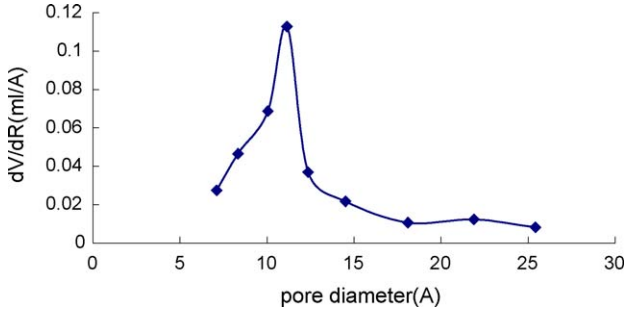

Fig. 3. Pore volume distribution curve of SiO_2–TiO_2 pillared montmorillonite.

3.4. UV–vis spectroscopy

Fig. 4 shows UV–vis diffuse reflectance spectrum of SiO_2–TiO_2 pillared clay. The absorption edge and the max were blue-shifted in comparison with that of anatase due to the quantum size effect of nanosized TiO_2 particles in the interlayered space of montmorillonite. Diffuse reflectance spectra of iron-doped SiO_2–TiO_2 pillared clay were not well resolved, indicating a large dispersion and disorder of Fe^{+3} species in the TiO_2 lattice and surface. All iron-doped samples show enhanced absorption in the range 350–500 nm, increasing higher for the more iron-charged samples. The red shift of the absorption edge of iron-doped SiO_2–TiO_2 pillared clay has been attributed to the excitation of 3d electrons of Fe^{+3} to the TiO_2 conduction band (charge–transfer transition [12,13], according to energy levels proposed [14]). The increased absorption in the range of 350–500 nm can be due also to transitions implicating surface states or native defects in the lattice.

3.5. Photocatalytic degradation of methyl orange

Fig. 5 shows the change of absorption spectrum of methyl orange in the suspension of SiO_2–TiO_2 PILC under the irradiation. The effect of the variation of photocatalyst amount can be seen on Fig. 6 and Table 1. The plot of ln C_o/C (where C_o is initial concentration of the methyl orange) with time of

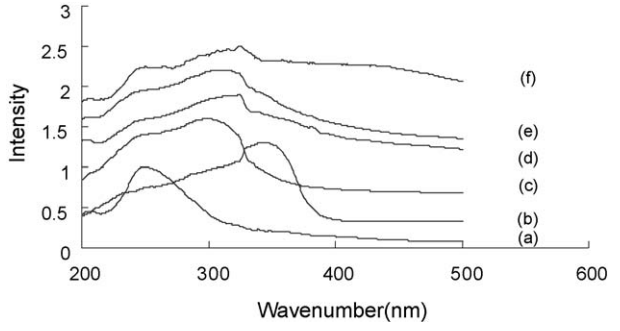

Fig. 4. Diffuse reflectance UV–vis spectra for (a) montmorillonite, (b) anatase, (c) PILC, (d) 0.448 Fe/PILC, (e) 1.792 Fe/PILC, and (f) 3.584 Fe/PILC.

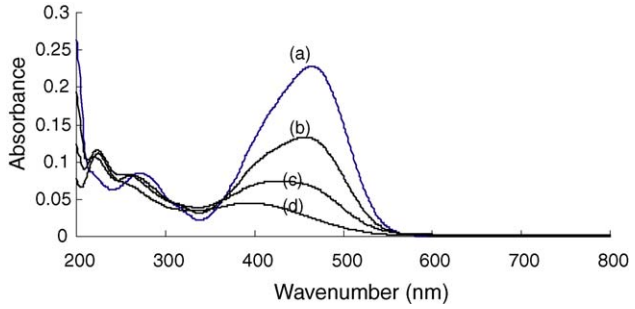

Fig. 5. The change of absorption spectra of methyl orange (0.01 mM) in the suspension of PILC (55 mg/l) under UV-light radiation in different irradiation time: (a) 0 h, (b) 2 h, (c) 4 h, and (d) 6 h.

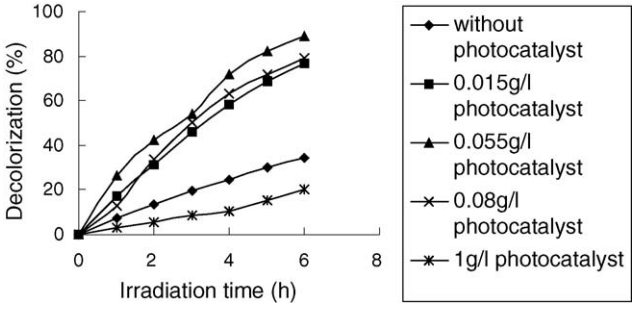

Fig. 6. Influence of the catalyst amount on the decolorization extent for methyl orange (0.01 mM).

irradiation (Fig. 7) shows that the photocatalytic decolorization of methyl orange is pseudo-first-order reaction. There is a limit (55 mg photocatalyst/l) above which no improvement is obtained by increasing the amount of catalyst. For higher quantities of photocatalyst, a screening effect of excess particles occurs, which masks part of the photosensitive surface. The similar observation had been made when investigating other dyes by other authors [15,16].

Table 1
Pseudo-first-order rate constant (k) for degradation of methyl orange in SiO_2–TiO_2 pillared montmorillonite suspension aqueous solution

Photocatalyst	Catalyst amount (g/l)	k (h^{-1})
PILC	0.015	0.094
PILC	0.055	0.132
PILC	0.08	0.107
THPILC	0.055	0.132
0.0056 Fe/PILC	0.055	0.127
0.0112 Fe/PILC	0.055	0.128
0.0224 Fe/PILC	0.055	0.124
0.0556 Fe/PILC	0.055	0.128
0.108 Fe/PILC	0.055	0.128
0.165 Fe/PILC	0.055	0.129
0.224 Fe/PILC	0.055	0.131
0.448 Fe/PILC	0.055	0.128
0.896 Fe/PILC	0.055	0.132
1.792 Fe/PILC	0.055	0.128
3.584 Fe/PILC	0.055	0.113

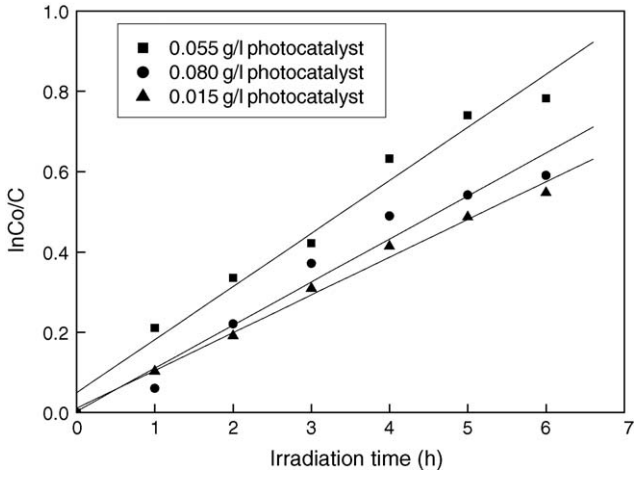

Fig. 7. Pseudo-first-order kinetics for decolorization of methyl orange.

Iron ions can introduce energy levels into the bandgap, which are responsible for the red-shift of intrinsic absorption edge of TiO_2 and of the enhancement of visible light adsorption, but there is no direct correlation between the light absorption ability and photocatalytic rate [17–27]. Factors related to the electronic structure seem to be more important, associated to the fact that dopant ions influence charge separation, charge–carrier recombination and interfacial charge–transfer rates, acting as mediators and affecting the quantum efficiencies. As a matter of fact, no visible light sensitized photoconductivity in 10 wt% iron-doped TiO_2 could be observed, in spite of the high absorbance of samples in this region [28].

Under irradiation, electron–hole pairs are produced in the conduction and valence bands of TiO_2, and successive events take place.

Charge-pair generation:

$$TiO_2 + h\nu \rightarrow e_{cb}^- + h_{vb}^+$$

Charge trapping:

$$Ti^{4+} + e_{cb}^- \rightarrow Ti^{3+}$$

$$> OH^- + h_{vb}^+ \rightarrow Ti^{4+} + OH^\bullet$$

Recombination:

$$e_{cb}^- + h_{vb}^+ \rightarrow TiO_2$$

$$Ti^{3+} + OH^\bullet \rightarrow Ti^{4+} + > OH^-$$

Interface electron transfer:

$$e_{cb}^-(Ti^{3+}) + Ox \rightarrow Ox^-$$

$$h_{vb}^+(OH^\bullet) + Red \rightarrow Red^+$$

where Ox is an electron acceptor and Red is electron donor. Irradiation of iron-doped TiO_2 can lead to the following addition steps.

Charge-pair generation:

$$Fe^{3+} + h\nu \rightarrow Fe^{4+} + e_{cb}{}^{-}$$

$$Fe^{3+} + h\nu \rightarrow Fe^{2+} + h_{vb}{}^{+}$$

Charge trapping:

$$Fe^{3+} + e^{-} \rightarrow Fe^{2+}$$

$$Fe^{3+} + h^{+} \rightarrow Fe^{4+}$$

Charge release and migration:

$$Fe^{2+} + Ti^{4+} \rightarrow Fe^{4+} + Ti^{3+}$$

$$Fe^{4+} + > OH^{-} \rightarrow Fe^{3+} + OH^{\bullet}$$

Recombination:

$$Fe^{2+} + h^{+} \rightarrow Fe^{3+}$$

$$Fe^{2+} + OH^{\bullet} \rightarrow Fe^{3+} + OH^{-}$$

$$Fe^{4+} + e^{-} \rightarrow Fe^{3+}$$

$$Fe^{4+} + Ti^{3+} \rightarrow Fe^{3+} + Ti^{4+}$$

Interfacial charge transfer:

$$e^{-}(Fe^{2+}) + Ox \rightarrow Ox^{-}$$

$$h^{+}(Fe^{4+}) + Red \rightarrow Red^{+}$$

It can be seen from Table 1 that presence of the iron ions does not influence or is detrimental on the photoreactivity. In iron-doped titania, Fe^{3+} can improve the photocatalytic efficiency by enhancing processes such as separation of photogenerated charges (by hole or electron trapping), detrapping and/or transfer of trapped charges to interface and to adsorbed substrates, reducing consequently recombination [17–27]. However, dopants can act as recombination centers too. The reduced activity can be explained because dopants act more as recombination centers than as trap sites for charge transfer at the interface, especially for samples with higher Fe^{3+} dopant concentration. In addition, an enhanced recombination is possible due to the rather low mobility of photoexcited electrons in iron oxide.

Finally, it should be remembered that all the SiO_2–TiO_2 pillared clay could be separated from the reacting system without filtration because they decant in several minutes.

4. Conclusion

Layered nanohybrid, which is one-to-one interstratified with a montmorillonite layer and a mixed SiO_2–TiO_2 sol particle one, has been prepared by ion exchange reaction of Na^+ ion in montmorillonite with the positively charged SiO_2–TiO_2 sol particles. Upon pillaring of oxide sols, the basal spacing of montmorillonite is expanded up to 46.5 nm. From nitrogen adsorption–desorption isotherm, the BET specific surface area and total porosity are found to be 446 m^2/g and 0.28 mg/l, respectively, and the pore size shows the value of ca. 1.1 nm. According to UV–vis spectra analysis, the blue-shift of the absorption edge was observed, indicating that the TiO_2 sol particles in the interlayer are quantum size. The photocatalytic decolorization of methyl orange is pseudo-first-order reaction. The presence of iron ion dopants did not beneficially influence the photoactivity of pillared clay for the photodegradation of methyl orange.

Acknowledgment

S. Liu is grateful for the fellowship under the Brain Pool program of Korea Federation of Science and Technology Society (KOSFT).

References

[1] M.R. Hoffmann, S.T. Martin, W. Choi, D.W. Bahnemann, Chem. Rev. 95 (1995) 69.
[2] Y.S. Han, S. Yamanaka, J.H. Choy, J. Solid State Chem. 144 (1999) 45.
[3] Z. Ding, H.Y. Zhu, P.F. Greenfield, J. Colloid Interface Sci. 209 (1999) 193.
[4] C. Ooka, S. Akita, Y. Ohashi, T. Horiuchi, K. Suzuki, S. Komai, H. Yoshida, T. Hattori, J. Mater. Chem. 9 (1999) 2943.
[5] C. Ooka, H. Yoshida, K. Suzuki, T. Hattori, Appl. Catal. A: Gen. 260 (2004) 47.
[6] C. Ooka, H. Yoshida, K. Suzuki, T. Hattori, Appl. Catal. B: Environ. 41 (2003) 313.
[7] J.H. Choy, J.H. Park, J.B. Yoon, J. Phys. Chem. B 108 (1998) 5991.
[8] S. Yamanaka, Y. Inoue, M. Hattori, F. Okumura, M. Yoshiikawa, Bull. Chem. Soc. Jpn. 65 (1992) 2494.
[9] K. Takahama, M. Yokoyama, S. Hirao, S. Yamanaka, S. Hattori, J. Mater. Sci. 27 (1992) 1297.
[10] S.J. Gregg, K.S. Sing, Adsorption Surface Area and Porosity, second ed., Academic Press, London, 1982.
[11] T. Allen, Particle Size Measurement, fourth ed., Chapman and Hall, London, 1980.
[12] J. Moser, M. Graztzel, R. Gallay, Helv. Chim. Acta 70 (1987) 1596.
[13] J.A. Navio, G. Colon, M.I. Litter, G.N. Bianco, J. Mol. Catal. A: Chem. 106 (1996) 267.
[14] K. Mizushima, M. Tanaka, A. Asai, S. Iida, J. Phys. Chem. Solids 40 (1979) 1129.
[15] M.S.T. Goncalves, A.M.F. Oliveira-Campos, E.M.M. Pinto, P.M.S. Plasencia, M.J.R.P. Queiroz, Chemosphere 39 (1999) 781.
[16] G. Ruppert, R. Bauer, Chemosphere 28 (1994) 1447.
[17] M.I. Litter, J.A. Navio, J. Photochem. Photobiol. A: Chem. 68 (1996) 171.
[18] W. Choi, A. Termin, M.R. Hoffmann, J. Phys. Chem. B 98 (1994) 13669.
[19] Z. Zhang, C. Wang, R. Zakaria, J.Y. Ying, J. Phys. Chem. B 102 (1998) 10871.
[20] M.R. Dhananjeyan, V. Kandavelu, R. Renganathan, J. Mol. Catal. A: Chem. 151 (2000) 217.
[21] C.Y. Wang, D.W. Bahnemann, J.K. Dohrmann, Chem. Commun. 16 (2000) 1539.

[22] R.I. Bickley, J.S. Lees, R.J.D. Tilley, L. Palmisano, S. Schiavello, J. Chem. Soc. Faraday Trans. 88 (1992) 377.
[23] W. Mu, J.M. Herrmann, P. Pichat, Catal. Lett. 3 (1989) 73.
[24] R.S. Sonawane, B.B. Kale, M.K. Dongare, Mater. Chem. Phys. 85 (2004) 52.
[25] V. Vamathevan, H. Tse, R. Amal, G. Low, S. McEvoy, Catal. Today 68 (2001) 201.
[26] M. Mrowetz, E. Selli, J. Photochem. Photobiol. A: Chem. 162 (2004) 89.
[27] J. Zhu, W. Zhang, B. He, J. Zhang, M. Anpo, J. Mol. Catal. A: Chem. 216 (2004) 35.
[28] N. Serpone, D. Lawless, J. Disdier, J.M. Herrmann, Langmuir 10 (1994) 643.